EDGE ARTICLE

Check for updates

Distinct hydrogen atom transfer and radical capture reactivity of copper(III) OH/F complexes enables site-selective C(sp³)−H ¹⁸F-fluorination

Joshua A. Queener,[a] Angela Asor,[b] Margaret A. P. Ball,[a] Jinghua Tang,[a] Jinda Fan*[bcd] and Shiyu Zhang [ID]*[a]

High-valent metal intermediates play a key role in C(sp³)−H functionalization reactions in both enzymatic catalysis and organometallic chemistry. Despite its generality, this strategy often requires a single metal complex to efficiently mediate both hydrogen atom transfer and radical capture—a combination challenging to achieve. To overcome this limitation, we propose a decoupled approach, where separate high-valent metal complexes independently perform hydrogen atom transfer (HAT) and radical capture (RC). As a proof of concept, we leveraged the complementary reactivity of copper(III) hydroxide (efficient for HAT) and copper(III) fluoride (efficient for RC) to develop a decoupled ¹⁸F-fluorination protocol. The distinct reactivity of copper(III) hydroxide and copper(III) fluoride not only enables precise control over the C−H activation process but also preserves the valuable [¹⁸F]fluoride for radical capture, preventing its consumption during HAT. With this mechanistic insight, we achieved the selective fluorination of α-ethereal, benzylic, and allylic C−H bonds, facilitating the synthesis of a series of ¹⁸F-labeled organic molecules.

High-valent metal complexes are prototypical intermediates in the activation and functionalization of C–H bonds.[1–4] Synthetic high-valent metal complexes featuring a diverse range of functional groups (M–FG, FG = functional groups), *e.g.*, hydroxide, superoxo, carboxylate, halides, nitrite, and nitrate, have been shown to activate alkyl C–H bonds.[5–14] In some cases, the M–FG complexes not only activate the C–H bond *via* hydrogen atom transfer (HAT) but also perform sequential radical capture (RC) to install the FG group on the C(sp³)–H position (Scheme 1A). For instance, studies by Tolman,[15–20] McDonald,[21–25] and our group,[26–28] have demonstrated that formal copper(III) and nickel(III) complexes can perform C–H halogenation, cyanation, and nitration. These transformations typically proceed with two equivalents of M–FG complexes – the first equivalent performs HAT, the second equivalent captures the R• generated from the first step (Scheme 1A).

Despite its generality, this strategy often requires a single metal complex to efficiently mediate both HAT and RC, a combination challenging to achieve. In many cases, the HAT and RC steps are not well synchronized, resulting in poor overall

C–H functionalization reactivity. For instance, the **LCuIII–F** (L = bis(2,6-diisopropylphenyl)pyridinedicarbox-amide) reported by us is efficient at RC, but the HAT process is sluggish, limiting

A C–H functionalization with high-valent metal complexes
Tolman, McDonald, Brudvig, Wang, Cho, Zhang, etc.

M = Mn, Fe, Co, Ni, Cu, etc. FG = OH, F, Cl, Br, NO₃, NO₂, O₂, CN

B Comparison of **LCuIII–OH** and **LCuIII–F**
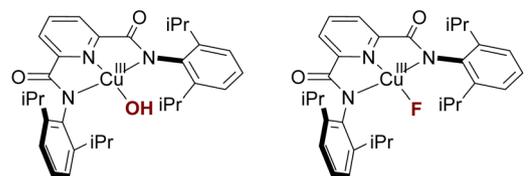
Tolman
Efficient for HAT
Inefficient for radical capture
No C–H hydroxylation

Zhang
Inefficient for HAT
Efficient for radical capture
Limited Substrate Scope

C Decoupled strategy for C–H functionalization with M-FG

Scheme 1

[a]Department of Chemistry and Biochemistry, The Ohio State University, Columbus, OH, 43210, USA. E-mail: zhang.8941@osu.edu

[b]Department of Chemistry, Michigan State University, East Lansing, MI, 48824, USA. E-mail: fanjinda@msu.edu

[c]Department of Radiology, Michigan State University, East Lansing, MI, 48824, USA

[d]Institute for Quantitative Health Science & Engineering, Michigan State University, East Lansing, MI, 48824, USA

the scope of C–H fluorination.[26,29] Conversely, the **LCu**[III]**–OH** complex reported by Tolman excels in HAT but is inefficient at RC, explaining why it has not been shown to perform C–H hydroxylation (Scheme 1B).

Another limitation is that functionalizing one equivalent of the C–H substrate requires two equivalents of the **LCu**[III]**–FG** complex, one for HAT and another for RC (Scheme 1A).[26,29] Consequently, applying this method to ^{18}F-fluorination (fluorine-18 is a short-lived radionuclide with $t_{1/2} = 109.7$ min) would result in the loss of one equivalent of valuable fluorine-18 for HAT.

To address these issues, we consider the possibility of a decoupled HAT and RC process, where HAT is performed with one high-valent metal complex (M–FG$_1$) and RC is performed with another (M–FG$_2$, Scheme 1C). To ensure that M–FG$_1$ and M–FG$_2$ perform their corresponding tasks without interfering with each other, it is essential to understand how the identity of the functional groups (FG$_1$ vs. FG$_2$) influences their relative rates and selectivity of HAT and RC.

As a proof-of-concept for this decoupled C–H functionalization strategy, we target the C–H ^{18}F-fluorination of the C(sp^3)–H bond. Organic molecules containing fluorine-18 are valuable for positron emission tomography (PET), a highly sensitive bioimaging technique used to diagnose cancers, neurological disorders, and cardiovascular diseases.[30–34] Traditional ^{18}F-labeling methods rely on the substitution of pre-existing functional groups with fluorine-18, e.g., I,[35–41] Cl,[42] Br,[43,44] S,[45,46] NR$_2$,[47,48] OR,[49–56] CO$_2$R,[57] BR$_2$,[58–63] and SnR$_3$.[64,65] However, recent efforts have shifted toward direct incorporation of fluorine-18 to C–H bonds.[66–68] Previous studies by Hooker, Groves,[6,8] Sanford, Scott,[35,69,70] Nicewicz, and Li[71,72] demonstrated the use of the readily available [^{18}F]fluoride anion for ^{18}F-fluorination of both C(sp^3)–H and C(sp^2)–H bonds (Scheme 2).

Despite these advancements, the selectivity of C(sp^3)–H ^{18}F-fluorination is often governed by the bond dissociation free energy (BDFE) of the C(sp^3)–H bonds[6,8] or the presence of a directing group.[35,69,70] Developing an alternative approach that

decouples the HAT and RC steps would allow for independent tuning of each process. This strategy could enable precise control over C–H activation through the steric and electronic properties of the metal complex, without compromising the efficiency of fluorine-18 atom transfer, ultimately providing alternative chemoselectivity in C–H ^{18}F-fluorination.

Herein, we investigate the distinct reactivity of **LCu**[III]**–OH** and **LCu**[III]**–F**. We found that **LCu**[III]**–OH** exhibits significantly higher efficiency in HAT (>400 times faster than **LCu**[III]**–F**), while **LCu**[III]**–F** demonstrates better performance in RC. Leveraging the contrasting reactivity of **LCu**[III]**–OH** and **LCu**[III]**–F**, we developed a ^{18}F-fluorination strategy, utilizing a simple mixture of **LCu**[III]**–OH** and **[**[18]**F]LCu**[III]**–F** complexes. This decoupled strategy allows tuning of C–H activation selectivity via steric control, polarity matching, and HAT asynchronicity,[27,29] without interfering with the efficiency of fluorine-18 atom transfer. We demonstrate the utility of this approach by labelling a broad range of C(sp^3)–H substrates, including pharmaceutical compounds, with fluorine-18, achieving C–H fluorination selectivity distinct from previously reported systems.

Our investigation began with the evaluation of the HAT rates of **LCu**[III]**–OH** and **LCu**[III]**–F** complexes. The copper(ii) precursors (**[LCu**[II]**–OH]**$^-$ and **[LCu**[II]**–F]**$^-$) have been isolated previously, and the corresponding copper(iii) species can be generated in situ using chemical oxidants, NAr$_3$[PF$_6$] (tris(p-bromophenylammoniumyl)hexafluorophosphate).[15,73] Addition of dihydroanthracene (DHA), a model hydrogen atom donor, to **LCu**[III]**–OH** or **LCu**[III]**–F** complexes at −30 °C led to the consumption of the copper complex, as revealed by UV-vis spectroscopy (Fig. 1A and B). The reaction between **LCu**[III]**–F** and DHA was confirmed to generate anthracene as the product, as evidenced by GC-MS analysis (Fig. S12–S14), indicating that the consumption of **LCu**[III]**–F** is due to HAT. Notably, Tolman et al. previously reported that the reaction of **LCu**[III]**–OH** with DHA also affords anthracene.[15] Therefore, it is reasonable to infer that both **LCu**[III]**–OH** and **LCu**[III]**–F** undergo the same HAT reaction mechanism with DHA under these conditions.

The second-order rate constants (k_{HAT}) were calculated by monitoring the decay of ligand-to-metal charge transfer (LMCT) bands of **LCu**[III]**–OH** (560 nm) and **LCu**[III]**–F** (820 nm, Fig. 1C) at varying equivalents of DHA. The **LCu**[III]**–OH** complex shows a HAT rate about 400 times faster than that of **LCu**[III]**–F** (0.04(1) vs. 0.0001(1) M^{-1} s^{-1}, Fig. 1C), suggesting that **LCu**[III]**–OH** would perform HAT preferentially in the presence of **LCu**[III]**–F**.

To confirm this hypothesis, we investigated the competitive HAT reactivity between **LCu**[III]**–OH** and **LCu**[III]**–F** in solution. Surprisingly, the addition of DHA to a 1 : 1 mixture of **LCu**[III]**–OH** and **LCu**[III]**–F** resulted in the consumption of both complexes at approximately equal rates (Fig. S15). This observation contrasts with our findings above that **LCu**[III]**–OH** exhibits a HAT rate 400 times faster than **LCu**[III]**–F** when the HAT reaction is evaluated in separate solutions. We attribute this apparent discrepancy to the fact that DHA donates two hydrogen atoms sequentially, with the second being more easily abstracted and transferred non-selectively, leading to concurrent consumption of both copper(iii) species.

A. Hooker and Groves

B. Sanford and Scott

C. Nicewicz and Li
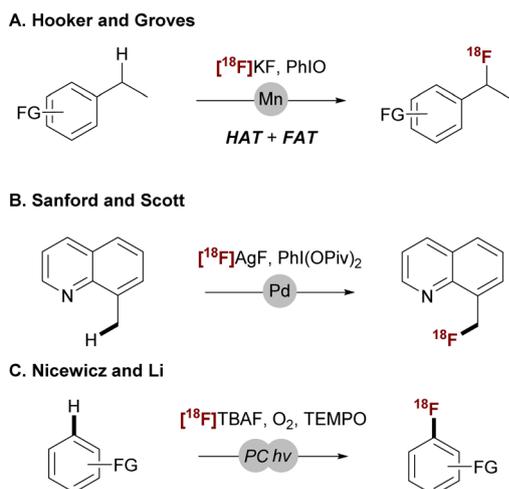
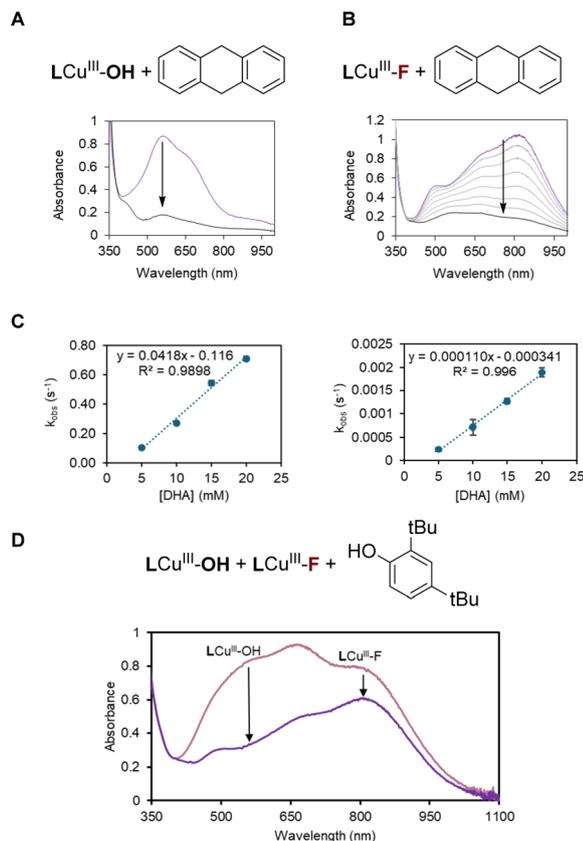**Scheme 2** C–H ^{18}F-fluorination using [^{18}F]F$^-$ sources.

Fig. 1 HAT kinetics of (A) LCu^{III}–OH and (B) LCu^{III}–F with 100 equivalents of DHA monitored by UV-vis spectrometry in dichloroethane at −30 °C. (C) The plots of k_{obs} (s^{-1}) for each complex with varying equivalents of DHA shows the faster HAT rate of LCu^{III}–OH than LCu^{III}–F. (D) UV-vis spectra of the reaction between the 1:1 mixture of LCu^{III}–OH and LCu^{III}–F with 1 equivalent of 2,4-di-*tert*-butylphenol monitored by UV-vis spectrometry in DCE at −30 °C after 1 minute.

To avoid complications from secondary H-atom transfer, we used 2,4-di-*tert*-butylphenol as the HAT donor in the competitive HAT studies. HAT from 2,4-di-*tert*-butylphenol yields phenoxy radicals that dimerize cleanly to form the C–C phenol dimer, allowing accurate evaluation of competitive HAT reactivity. Indeed, GC-MS analysis confirmed that both LCu^{III}–OH and LCu^{III}–F oxidize 2,4-di-*tert*-butylphenol to produce the phenol dimer (3,3′,5,5′-tetra(*tert*-butyl)biphenyl-2,2′-diol), as the main product (see the SI).

When a 1:1 mixture of LCu^{III}–OH and LCu^{III}–F is treated with one equivalent of hydrogen atom donor, 2,4-di-*tert*-butyl-phenol (chosen as a simple single H atom donor), only 5% of LCu^{III}–F is consumed before the complete consumption of all LCu^{III}–OH, validating the selective HAT activity by LCu^{III}–OH under these conditions (Fig. 1D). Additionally, UV-vis analysis of a 1:1 mixture of LCu^{III}–OH and LCu^{III}–F indicates that the two species coexist without detectable side reactions, such as ligand exchange or disproportionation.

Next, we evaluated if LCu^{III}–F can capture C-centered radicals to form the desired C–F bonds without interference from LCu^{III}–OH. We compared the RC capability of LCu^{III}–OH and
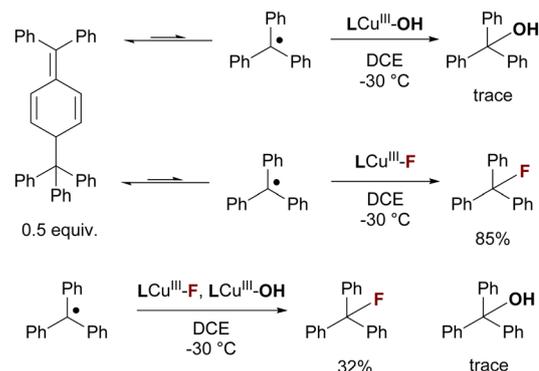
Scheme 3 Selectivity of radical capture with LCu^{III}–FG.

Scheme 4 Procedure for ^{18}F labeling.

LCu^{III}–F by treating them with 0.5 equivalent of Gomberg's dimer (Scheme 3), which can dissociate into the trityl radical (Ph$_3$C$^•$) in solution, serving as a model for C-centered radicals. The yield of the radical capture product (Ph$_3$C–F) was found to be 85% by ^{19}F NMR, while only a trace amount (<1%) of the hydroxide transferred product (Ph$_3$C–OH) was observed by GC-MS (see the SI). When a 1:1 mixture of LCu^{III}–OH and LCu^{III}–F was treated with 0.5 equivalent of Gomberg's dimer (Scheme 3), the yield of the fluorine atom transfer (FAT) product (Ph$_3$C–F) was found to be 32% by ^{19}F NMR, and again only a trace amount (<1%) of the hydroxide transferred product (Ph$_3$C–OH) was observed by GC-MS (see the SI). The reason for the reduced yield of Ph$_3$C–F in the presence of LCu^{III}–OH is unclear to us. However, the much higher yield of Ph$_3$C–F than Ph$_3$C–OH suggests that LCu^{III}–F might preferentially capture the alkyl radical generated from HAT. The higher radical capture efficiency observed for LCu^{III}–F compared to LCu^{III}–OH can be attributed to the higher redox potential of LCu^{III}–F (216.4 mV vs. Fc$^+$/Fc). Because alkyl

Table 1 Optimization of ^{18}F C−H fluorination conditions

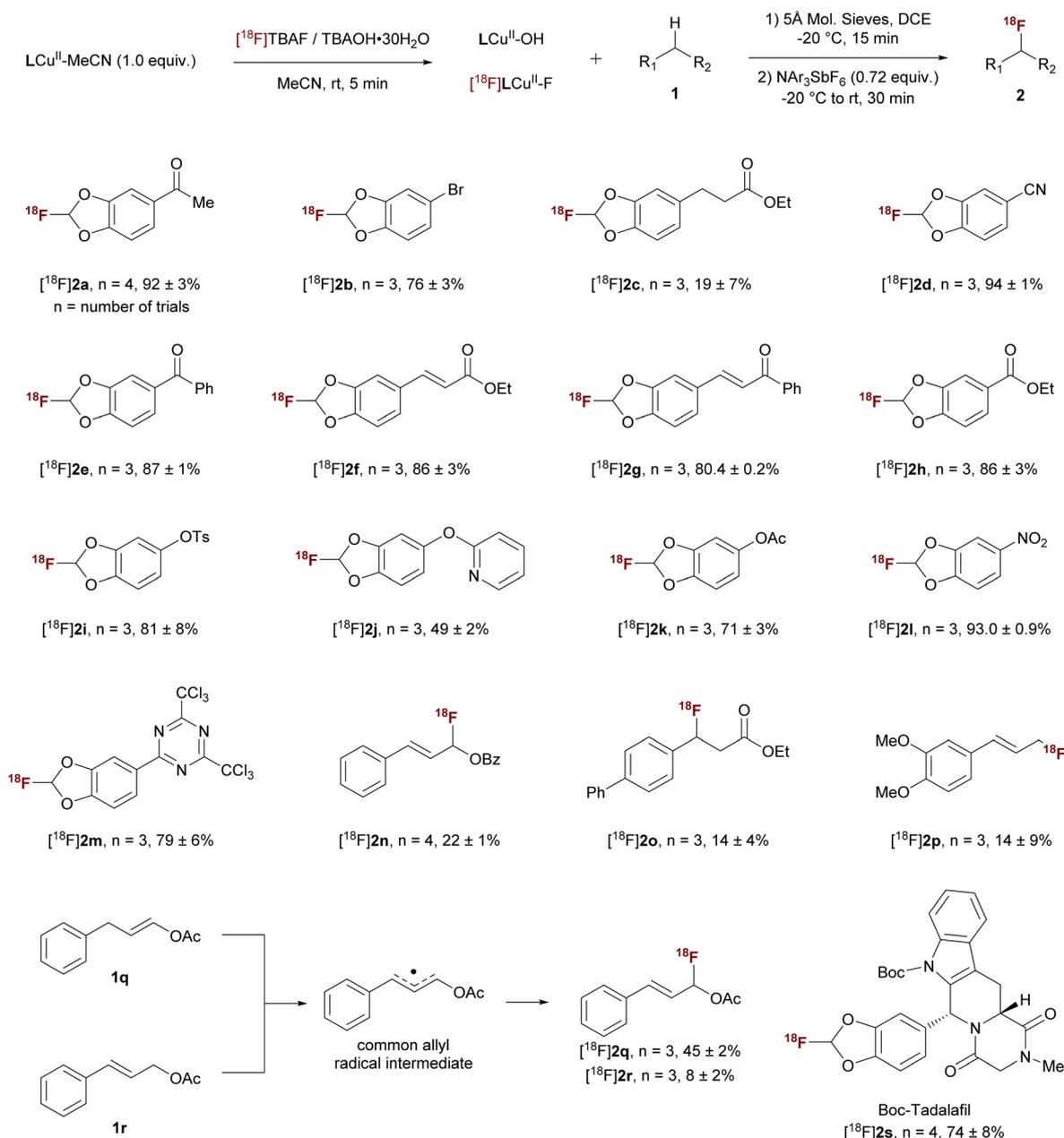| Entry	Deviation from standard conditions	RCC
1	None	92%
2	No 5 Å MS	18%
3	1.0 equiv. of substrate	23%
4	0.72 equiv. NAr$_3$[PF$_6$]	86%
5	1.0 equiv. NAr$_3$[PF$_6$]	25%

radical capture is proposed to proceed *via* an electron transfer–halide transfer mechanism, the higher redox potential of **LCu**^{III}**–F** facilitates oxidation of the alkyl radical and thus promotes efficient radical capture, whereas the lower redox potential of **LCu**^{III}**–OH** (−135.2 mV *vs.* Fc$^+$/Fc) renders it much less effective.[74]

After establishing that **LCu**^{III}**–OH** and **LCu**^{III}**–F** can perform HAT and RC, respectively, we set out to develop a method that combines the HAT and RC steps to achieve C(sp^3)–H ^{18}F-fluorination (Scheme 4). First, we passed an acetonitrile solution of TBAOH·30H$_2$O through an ion-exchange cartridge

loaded with [^{18}F]F$^-$ (*ca.* 0.11 GBq, 3 mCi) to generate a mixture of TBAOH and [^{18}F]TBAF.

Treatment of the solution mixture of TBAOH and [^{18}F]TBAF with one equivalent of **LCu**^{II}**–MeCN** (with respect to the total TBA concentration) led to a color change to dark blue, consistent with the formation of a mixture of [**LCu**^{II}**–OH**]$^-$ and [^{18}F][**LCu**^{II}**–F**]$^-$. A full equivalent of **LCu**^{II}**–MeCN**, with respect to the total concentration of TBAOH and TBAF, was added to ensure that all nucleophilic ligands (OH$^-$ and [^{18}F]F$^-$) are properly ligated, thereby preventing competitive displacement of [^{18}F]F$^-$ with OH$^-$. This mixture was oxidized to the copper(III) state using NAr$_3$[PF$_6$] ($E_{1/2}$ = 0.710 V *vs.* Fc/Fc$^+$ in dichloroethane

---

Table 2 Substrate scope for ^{18}F C–H fluorination

[^{18}F]**2a**, n = 4, 92 ± 3%
n = number of trials

[^{18}F]**2b**, n = 3, 76 ± 3%

[^{18}F]**2c**, n = 3, 19 ± 7%

[^{18}F]**2d**, n = 3, 94 ± 1%

[^{18}F]**2e**, n = 3, 87 ± 1%

[^{18}F]**2f**, n = 3, 86 ± 3%

[^{18}F]**2g**, n = 3, 80.4 ± 0.2%

[^{18}F]**2h**, n = 3, 86 ± 3%

[^{18}F]**2i**, n = 3, 81 ± 8%

[^{18}F]**2j**, n = 3, 49 ± 2%

[^{18}F]**2k**, n = 3, 71 ± 3%

[^{18}F]**2l**, n = 3, 93.0 ± 0.9%

[^{18}F]**2m**, n = 3, 79 ± 6%

[^{18}F]**2n**, n = 4, 22 ± 1%

[^{18}F]**2o**, n = 3, 14 ± 4%

[^{18}F]**2p**, n = 3, 14 ± 9%

common allyl radical intermediate

[^{18}F]**2q**, n = 3, 45 ± 2%
[^{18}F]**2r**, n = 3, 8 ± 2%

Boc-Tadalafil
[^{18}F]**2s**, n = 4, 74 ± 8%

DCE) and then transferred to a DCE solution containing C–H substrates at −20 °C for C–H ^{18}F-fluorination.

Excitingly, we found that the model C–H substrate 1,3-benzodioxole (**1a**) was converted to the ^{18}F-labeled product in 92% radiochemical conversion (RCC, average of four trials, $n = 4$) under the optimized conditions (Table 1). The entire procedure can be completed within an hour (Scheme 4). The radiochemical conversions were determined by radio-TLC analysis of the reaction mixtures. The identity of the ^{18}F-labeled product was confirmed by comparing the retention time of the ^{18}F-labeled products with the corresponding ^{19}F standards using radio-HPLC (see the SI). The present Cu method also proceeds under ^{19}F conditions; however, due to difficulties in separating the fluorinated product from the unreacted starting material, an alternative method using a stoichiometric amount of C–H substrates was developed for isolating the ^{19}F standards (see the SI).

The reaction is sensitive to the water introduced by TBAOH·30H$_2$O. Without 5 Å molecular sieves as a desiccant, the yield of the reaction drops to 18% (entry 2). Moreover, the use of 0.72 equivalent instead of one equivalent of oxidant (with respect to total copper(II) concentration) affords the highest radiochemical yield, likely by minimizing oxidation of the fluorinated product. Finally, switching from a PF$_6$-based oxidant to an SbF$_6$-based oxidant affords more consistent radiochemical yields.

Under the optimal conditions, the substrate scope of C–H fluorination was investigated. As summarized in Table 2, a wide range of 1,3-benzodioxole C–H substrates can be converted to fluorinated products with high RCY. The reaction conditions tolerate many common functional groups, including enolizable ketones (**2a**), aryl halides (**2b**), esters (**2c**, **2f**, and **2h**), heterocycles (**2j**, **2m**, and **2s**), and cyano (**2d**) and nitro (**2l**) groups. Additionally, benzylic and allylic C–H substrates can be fluorinated with various efficiencies (**2n–2r**). Interestingly, substrates **1q** and **1r** yield the same product through a delocalized allyl radical intermediate, suggesting radical capture selectively occurs at the less sterically hindered position. The potential utility of this method is further demonstrated through the ^{18}F-fluorination of Boc-Tadalafil in 74% RCC (**2s**, Table 2). Although the mono-fluorinated benzodioxole motif is readily accessible *via* our ^{18}F-labeling methodology, preliminary stability studies indicate that certain derivatives (*e.g.*, **2d** and **2s**) are prone to hydrolysis under acidic, basic, and simulated physiological conditions (see the SI). These findings highlight that while the labelling method itself is robust and versatile, the hydrolytic and metabolic instability of some derivatives may limit their direct *in vivo* application. Nevertheless, the methodology provides a general platform to access these fluorinated motifs, which can guide future efforts to design derivatives with enhanced stability for biological imaging applications. As a proof of concept, ^{18}F-labeled **2d** was isolated with preparative HPLC with 14.5% decay corrected RCY and a molar activity of 1.22 ± 0.42 GBq μmol^{-1} EOS (end of synthesis, Fig. S23–S25).

To confirm that the C–H fluorination of 1,3-benzodioxoles still proceeds through the proposed HAT/radical rebound mechanism. We performed a kinetic isotope effect (KIE) study

of the reaction between **LCu^{III}–OH/F** and **1a** and 3,4-methyl-enedioxyacetophenone-d_2 (**1a-d_2**). The KIE values were found to be 11.8 ± 1.8 and 2.95 ± 0.68 for **LCu^{III}–OH** and **LCu^{III}–F**, respectively. These results suggest that the activation of the C–H bond *via* proton-coupled electron transfer (PCET) is the rate-limiting step for both copper complexes.

Notably, **1s** contains both a 1,3-benzodioxole motif (Fig. 2B, H$_\gamma$) and other weak benzylic C–H bonds (H$_\alpha$ and H$_\beta$), but only the 1,3-benzodioxole C–H bond (C–H$_\gamma$) was activated. This selectivity contrasts the report by Groves *et al.* using manganese(v) oxo fluoride species, which favors C–H positions with low BDFE (Fig. 2A).[6,8] We attribute this unique selectivity to the selective HAT step by **LCu^{III}–OH**, since HAT is the rate-limiting step as previously reported.[73] The **LCu^{III}–OH** preferentially activates electron-rich C(sp^3)–H bonds due to polarity matching. Specifically, the electrophilic nature of formal copper(III) complexes accelerates C–H activation *via* asynchronous PCET.[27,29,76,77]

To evaluate this hypothesis, we calculated the PCET asynchronicity factor η of various C–H substrates using density functional theory (DFT, see the SI).[75–77] The DFT-computed η factor shows that PCET from electron-rich benzylic substrates and 1,3-benzodioxole to **LCu^{III}–OH** is highly oxidative and asynchronous (1.445–1.553 V), which is expected to increase the rates of HAT.

We apply this rationale to explain the C–H fluorination selectivity on Boc-Tadalafil **1s**, which contains both benzylic (H$_\alpha$ and H$_\beta$) and α-ethereal C–H bonds (H$_\gamma$). The calculated BDFE of C$_\alpha$–H, C$_\beta$–H, and C$_\gamma$–H shows that the C$_\gamma$–H bond is the strongest (90 kcal mol^{-1}). However, the copper(III) system still selectively fluorinates C$_\gamma$–H over C$_\alpha$–H (83 kcal mol^{-1}) and C$_\beta$–H (78 kcal mol^{-1}) positions (Fig. 2B). This unconventional C–H functionalization selectivity can be explained by the contribution of polarity matching to the barrier of PCET through
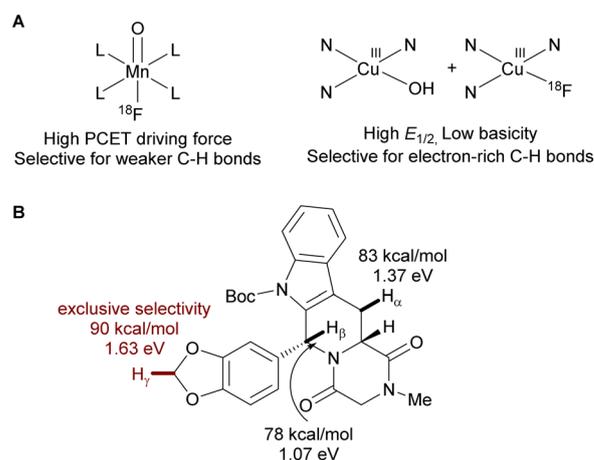
Fig. 2 (A) Comparison of selectivity of the O=Mn^V–F system reported by Groves *et al.* and the Cu^{III} system reported in this work. The selectivity of the O=Mn^V–F system is dictated by the bond dissociation free energy (BDFE) values of the C–H substrate, while the selectivity of Cu^{III}–OH is dictated by the asynchronicity of PCET. (B) Calculated BDFE and asynchronicity factors for three potential C–H fluorination sites.

asynchronicity (η), where the greater the asynchronicity the lower the activation barrier. The distinct C–H fluorination selectivity observed here, compared to the work of Groves and Hooker, underscores how new organometallic reagents can expand the scope of C–H ^{18}F-fluorination, thereby enhancing the structural diversity of ^{18}F-radiotracers.

In summary, we developed a novel ^{18}F-labeling methodology through the tandem use of copper(III) hydroxide as a HAT mediator and copper(III) fluoride as a FAT agent with high RCCs of up to 94%. The decoupled HAT and FAT reactivity of copper(III) complexes allows for the activation and fluorination of electron-rich C–H bonds, which are not normally accessible by traditional C–H fluorination methods, which favor C–H bonds with low BDFE, such as benzylic and allylic positions. The tandem use of the HAT reagent and fluorine source, in principle, can provide further practicality and generality to C(sp^3)–H ^{18}F-fluorination, *i.e.*, regioselectivity and stereoselectivity. This will be the subject of our future study.

Author contributions

S. Z. and J. F. conceived the main idea of the project. J. A. Q., A. A., M. A. P. B., J. T. designed the experiment and performed the data analyses. J. A. Q., S. Z., and J. F. prepared the manuscript.

Conflicts of interest

There are no conflicts to declare.

Data availability

The datasets supporting this article have been uploaded as part of the supplementary information (SI), including synthesis and characterization information, spectroscopic data, and DFT calculations. Supplementary information is available. See DOI: https://doi.org/10.1039/d5sc06381g.

Acknowledgements

Notes and references

1 A. Gunay and K. H. Theopold, *Chem. Rev.*, 2010, **110**, 1060–1081.
2 W. Liu and J. T. Groves, *Acc. Chem. Res.*, 2015, **48**, 1727–1735.
3 M. Puri, A. N. Biswas, R. Fan, Y. Guo and L. Que, *J. Am. Chem. Soc.*, 2016, **138**, 2484–2487.
4 A. S. Borovik, *Chem. Soc. Rev.*, 2011, **40**, 1870–1874.
5 W. Liu and J. T. Groves, *Angew. Chem., Int. Ed.*, 2013, **52**, 6024–6027.
6 X. Huang, W. Liu, H. Ren, R. Neelamegam, J. M. Hooker and J. T. Groves, *J. Am. Chem. Soc.*, 2014, **136**, 6842–6845.
7 W. Liu, X. Huang, M.-J. Cheng, R. J. Nielsen, W. A. Goddard and J. T. Groves, *Science*, 2012, **337**, 1322–1325.
8 W. Liu, X. Huang, M. S. Placzek, S. W. Krska, P. McQuade, J. M. Hooker and J. T. Groves, *Chem. Sci.*, 2018, **9**, 1168–1172.
9 G. Li, A. K. Dilger, P. T. Cheng, W. R. Ewing and J. T. Groves, *Angew. Chem., Int. Ed.*, 2018, **57**, 1251–1255.
10 C. Panda, O. Anny-Nzekwue, L. M. Doyle, R. Gericke and A. R. McDonald, *JACS Au*, 2023, **3**, 919–928.
11 T. Corona, A. Draksharapu, S. K. Padamati, I. Gamba, V. Martin-Diaconescu, F. Acuna-Parés, W. R. Browne and A. Company, *J. Am. Chem. Soc.*, 2016, **138**, 12987–12996.
12 K. J. Fisher, M. L. Feuer, H. M. C. Lant, B. Q. Mercado, R. H. Crabtree and G. W. Brudvig, *Chem. Sci.*, 2020, **11**, 1683–1690.
13 Y. M. Kwon, Y. Lee, G. E. Evenson, T. A. Jackson and D. Wang, *J. Am. Chem. Soc.*, 2020, **142**, 13435–13441.
14 D. Jeong, Y. Lee, Y. Lee, K. Kim and J. Cho, *J. Am. Chem. Soc.*, 2024, **146**, 4172–4177.
15 P. J. Donoghue, J. Tehranchi, C. J. Cramer, R. Sarangi, E. I. Solomon and W. B. Tolman, *J. Am. Chem. Soc.*, 2011, **133**, 17602–17605.
16 D. Dhar and W. B. Tolman, *J. Am. Chem. Soc.*, 2015, **137**, 1322–1329.
17 D. Dhar, G. M. Yee, A. D. Spaeth, D. W. Boyce, H. Zhang, B. Dereli, C. J. Cramer and W. B. Tolman, *J. Am. Chem. Soc.*, 2016, **138**, 356–368.
18 C. E. Elwell, M. Mandal, C. J. Bouchey, L. Que, C. J. Cramer and W. B. Tolman, *Inorg. Chem.*, 2019, **58**, 15872–15879.
19 M. Mandal, C. E. Elwell, C. J. Bouchey, T. J. Zerk, W. B. Tolman and C. J. Cramer, *J. Am. Chem. Soc.*, 2019, **141**, 17236–17244.
20 C. J. Bouchey and W. B. Tolman, *Inorg. Chem.*, 2022, **61**, 2662–2668.
21 P. Pirovano, E. R. Farquhar, M. Swart and A. R. McDonald, *J. Am. Chem. Soc.*, 2016, **138**, 14362–14370.
22 P. Mondal, P. Pirovano, A. Das, E. R. Farquhar and A. R. McDonald, *J. Am. Chem. Soc.*, 2018, **140**, 1834–1841.
23 D. Unjaroen, R. Gericke, M. Lovisari, D. Nelis, P. Mondal, P. Pirovano, B. Twamley, E. R. Farquhar and A. R. Mcdonald, *Inorg. Chem.*, 2019, **58**, 16838–16848.
24 P. Mondal, M. Lovisari, B. Twamley and A. R. McDonald, *Angew. Chem., Int. Ed.*, 2020, **59**, 13044–13050.
25 C. Panda, L. M. Doyle, R. Gericke and A. R. McDonald, *Angew. Chem., Int. Ed.*, 2021, **60**, 26281–26286.
26 J. K. Bower, A. D. Cypcar, B. Henriquez, S. C. E. Stieber and S. Zhang, *J. Am. Chem. Soc.*, 2020, **142**, 8514–8521.
27 J. K. Bower, M. S. Reese, I. M. Mazin, L. M. Zarnitsa, A. D. Cypcar, C. E. Moore, A. Y. Sokolov and S. Zhang, *Chem. Sci.*, 2023, **14**, 1301–1307.
28 M. A. P. Ball, P. J. Myers, G. D. Ritch, J. K. Bower, C. E. Moore, N. K. Szymczak and S. Zhang, *Angew. Chem., Int. Ed.*, 2024, e202420677.
29 H. Hintz, J. Bower, J. Tang, M. LaLama, C. Sevov and S. Zhang, *Chem Catal.*, 2023, **3**, 100491.
30 J. Rong, A. Haider, T. E. Jeppesen, L. Josephson and S. H. Liang, *Nat. Commun.*, 2023, **14**, 3257.

31 S. Preshlock, M. Tredwell and V. Gouverneur, *Chem. Rev.*, 2016, **116**, 719–766.

32 M. G. Campbell, J. Mercier, C. Genicot, V. Gouverneur, J. M. Hooker and T. Ritter, *Nat. Chem.*, 2017, **9**, 1–3.

33 V. W. Pike, *Trends Pharmacol. Sci.*, 2009, **30**, 431–440.

34 S. M. Ametamey, M. Honer and P. August Schubiger, *Chem. Rev.*, 2008, **108**, 1501–1516.

35 M. S. McCammant, S. Thompson, A. F. Brooks, S. W. Krska, P. J. H. Scott and M. S. Sanford, *Org. Lett.*, 2017, **19**, 3939–3942.

36 N. Ichiishi, A. F. Brooks, J. J. Topczewski, M. E. Rodnick, M. S. Sanford and P. J. H. Scott, *Org. Lett.*, 2014, **16**, 3224–3227.

37 T. E. Spiller, K. Donabauer, A. F. Brooks, J. A. Witek, G. D. Bowden, P. J. H. Scott and M. S. Sanford, *Org. Lett.*, 2024, **26**, 6433–6437.

38 M. B. Haskali, S. Telu, Y.-S. Lee, C. L. Morse, S. Lu and V. W. Pike, *J. Org. Chem.*, 2015, **81**, 297–302.

39 J.-H. Chun, S. Lu, Y.-S. Lee and V. W. Pike, *J. Org. Chem.*, 2010, **75**, 3332–3338.

40 T. L. Ross, J. Ermert, C. Hocke and H. H. Coenen, *J. Am. Chem. Soc.*, 2007, **129**, 8018–8025.

41 S. Calderwood, T. L. Collier, V. Gouverneur, S. H. Liang and N. Vasdev, *J. Fluorine Chem.*, 2015, **178**, 249–253.

42 W. Chen, H. Wang, N. E. S. Tay, V. A. Pistritto, K. Li, T. Zhang, Z. Wu, D. A. Nicewicz and Z. Li, *Nat. Chem.*, 2022, **14**, 216–223.

43 L. S. Sharninghausen, A. F. Brooks, W. P. Winton, K. J. Makaravage, P. J. H. Scott and M. S. Sanford, *J. Am. Chem. Soc.*, 2020, **142**, 7362–7367.

44 E. Lee, J. M. Hooker and T. Ritter, *J. Am. Chem. Soc.*, 2012, **134**, 17456–17458.

45 P. Xu, D. Zhao, F. Berger, A. Hamad, J. Rickmeier, R. Petzold, M. Kondratiuk, K. Bohdan and T. Ritter, *Angew. Chem., Int. Ed.*, 2020, **59**, 1956–1960.

46 L. Mu, C. R. Fischer, J. P. Holland, J. Becaud, P. A. Schubiger, R. Schibli, S. M. Ametamey, K. Graham, T. Stellfeld, L. M. Dinkelborg and L. Lehmann, *Eur. J. Org. Chem.*, 2012, 889–892.

47 R. M. Pérez-García, G. Grønnevik and P. J. Riss, *Org. Lett.*, 2021, **23**, 1011–1015.

48 E. E. Gray, M. K. Nielsen, K. A. Choquette, J. A. Kalow, T. J. A. Graham and A. G. Doyle, *J. Am. Chem. Soc.*, 2016, **138**, 10802–10805.

49 T. J. A. Graham, R. Frederick Lambert, K. Ploessl, H. F. Kung and A. G. Doyle, *J. Am. Chem. Soc.*, 2014, **136**, 5291–5294.

50 M. K. Nielsen, C. R. Ugaz, W. Li and A. G. Doyle, *J. Am. Chem. Soc.*, 2015, **137**, 9571–9574.

51 C. N. Neumann, J. M. Hooker and T. Ritter, *Nature*, 2016, **534**, 369–373.

52 H. Beyzavi, D. Mandal, M. G. Strebl, C. N. Neumann, E. M. D'Amato, J. Chen, J. M. Hooker and T. Ritter, *ACS Cent. Sci.*, 2017, **3**, 944–948.

53 N. E. S. Tay, W. Chen, A. Levens, V. A. Pistritto, Z. Huang, Z. Wu, Z. Li and D. A. Nicewicz, *Nat. Catal.*, 2020, **3**, 734–742.

54 J. J. Topczewski, T. J. Tewson and H. M. Nguyen, *J. Am. Chem. Soc.*, 2011, **133**, 19318–19321.

55 S. Ortalli, J. Ford, A. A. Trabanco, M. Tredwell and V. Gouverneur, *J. Am. Chem. Soc.*, 2024, **146**, 11599–11604.

56 R. Halder, G. Ma, J. Rickmeier, J. W. McDaniel, R. Petzold, C. N. Neumann, J. M. Murphy and T. Ritter, *Nat. Protoc.*, 2023, **18**, 3614–3651.

57 E. W. Webb, J. B. Park, E. L. Cole, D. J. Donnelly, S. J. Bonacorsi, W. R. Ewing and A. G. Doyle, *J. Am. Chem. Soc.*, 2020, **142**, 9493–9500.

58 A. V. Mossine, A. F. Brooks, K. J. Makaravage, J. M. Miller, N. Ichiishi, M. S. Sanford and P. J. H. Scott, *Org. Lett.*, 2015, **17**, 5780–5783.

59 J. S. Wright, L. S. Sharninghausen, S. Preshlock, A. F. Brooks, M. S. Sanford and P. J. H. Scott, *J. Am. Chem. Soc.*, 2021, **143**, 6915–6921.

60 S. Preshlock, S. Calderwood, S. Verhoog, M. Tredwell, M. Huiban, A. Hienzsch, S. Gruber, T. C. Wilson, N. J. Taylor, T. Cailly, M. Schedler, T. L. Collier, J. Passchier, R. Smits, J. Mollitor, A. Hoepping, M. Mueller, C. Genicot, J. Mercier and V. Gouverneur, *Chem. Commun.*, 2016, **52**, 8361–8364.

61 A. J. Hoover, M. Lazari, H. Ren, M. K. Narayanam, J. M. Murphy, R. M. Van Dam, J. M. Hooker and T. Ritter, *Organometallics*, 2016, **35**, 1008–1014.

62 M. Tredwell, S. M. Preshlock, N. J. Taylor, S. Gruber, M. Huiban, J. Passchier, J. Mercier, C. Génicot and V. Gouverneur, *Angew. Chem., Int. Ed.*, 2014, **53**, 7751–7755.

63 V. Orlovskaya, O. Fedorova, O. Kuznetsova and R. Krasikova, *Eur. J. Org. Chem.*, 2020, **2020**, 7079–7086.

64 H. Teare, E. G. Robins, A. Kirjavainen, S. Forsback, G. Sandford, O. Solin, S. K. Luthra and V. Gouverneur, *Angew. Chem., Int. Ed.*, 2010, **49**, 6821–6824.

65 K. J. Makaravage, A. F. Brooks, A. V. Mossine, M. S. Sanford and P. J. H. Scott, *Org. Lett.*, 2016, **18**, 5440–5443.

66 R. Szpera, D. F. J. Moseley, L. B. Smith, A. J. Sterling and V. Gouverneur, *Angew. Chem., Int. Ed.*, 2019, **58**, 14824–14848.

67 X. Yang, T. Wu, R. J. Phipps and F. D. Toste, *Chem. Rev.*, 2015, **115**, 826–870.

68 Y. Zhou, J. Wang, Z. Gu, S. Wang, W. Zhu, J. Luis Aceña, V. A. Soloshonok, K. Izawa and H. Liu, *Chem. Rev.*, 2016, **116**, 422–518.

69 S. J. Lee, K. J. Makaravage, A. F. Brooks, P. J. H. Scott and M. S. Sanford, *Angew. Chem., Int. Ed.*, 2019, **58**, 3119–3122.

70 S. J. Lee, A. F. Brooks, N. Ichiishi, K. J. Makaravage, A. V. Mossine, M. S. Sanford and P. J. H. Scott, *Chem. Commun.*, 2019, **55**, 2976–2979.

71 W. Chen, Z. Huang, N. E. S. Tay, B. Giglio, M. Wang, H. Wang, Z. Wu, D. A. Nicewicz and Z. Li, *Science*, 2019, **364**, 1170–1174.

72 L. Wang, A. R. White, W. Chen, Z. Wu, D. A. Nicewicz and Z. Li, *Org. Lett.*, 2020, **22**, 7971–7975.

73 J. K. Bower, A. D. Cypcar, B. Henriquez, S. C. E. Stieber and S. Zhang, *J. Am. Chem. Soc.*, 2020, **142**, 8514–8521.

74 J. K. Kochi, *Science*, 1967, **155**, 415–424.

75 B. Daniel, M.-D. Mauricio, R. Lubomír, S. Martin, D. Bím, M. Maldonado-Domínguez, L. Rulíšek and M. Srnec, *Proc. Natl. Acad. Sci. U. S. A.*, 2018, **115**, E10287–E10294.

76 S. K. Barman, M. Y. Yang, T. H. Parsell, M. T. Green and A. S. Borovik, *Proc. Natl. Acad. Sci. U. S. A.*, 2021, **118**, e2108648118.

77 M. K. Goetz and J. S. Anderson, *J. Am. Chem. Soc.*, 2019, **141**, 4051–4062.